Le Evaluation of an InP Mach-Zehnder modulator for high speed optical network system architectures and emerging photonically integrated optical modules

P. MITCHELL[ab], R. LONGONE[a], A. JANSSEN[a], B. GARRETT[a], J. K. LUO[b]
[a]Oclaro Technology, Paignton, Devon, TQ47AU, UK.
[b]Centre for Material Research & Innovation, University of Bolton, Deane Road, Bolton, BL35AB, UK.

The realization of an Indium Phosphide material based Multi Quantum Well Mach-Zehnder modulator (InP MZ) provides many advantages compared to other contemporary optical modulator technologies available. Utilizing the Quantum Confined Stark Effect (QCSE) in a semiconductor Multi Quantum Well (MQW) it enables a small physical size modulator to be realized with comparatively low drive voltage and low power consumption. The development of a equivalent InP MZ model enables optical systems performance to be simulated and is a very important tool for system architects as part of a technology evaluation activity, enabling the performance of an optical component incorporating the InP MZ to be evaluated and overall systems performance and ultimate network topology to be quantified prior to committing financial expense and other resources. This paper discusses the realization of the model following a detailed analysis of the InP MZ modulator characteristics. A comparison of the simulated versus practical results of a fabricated InP MZ is presented.

1. Introduction

The demands on modern optical network infrastructures continue to rise. Driven through the increase in triple play services such as voice, broadband and video on demand, these new services are driving new layer 1 and layer 2 technologies along with the convergence of IP services over Ethernet transport. The continued evolution of optical component technologies such as optical modulators supports the emerging network systems and is an enabler for enhanced network performance and reduced overall cost. The Lithium Niobate (LiNbO$_3$) Mach-Zehnder (MZ) modulator is well established and is currently the most popular high speed optical modulator to date. LiNbO$_3$ has been selected as the material of choice for fabrication of electro-optic devices due to its combination of high electro-optic coefficients and high optical transparency (low loss) in the near infrared wavelengths. This modulator is currently the bench mark of all MZ modulator architectures, although physically long, ~50mm in length, it has established itself as a modulator of high reliability & high performance since its introduction in the 1980s [1, 2]. Indium Phosphide (InP) Multi Quantum Well (MQW) MZ modulator is an emerging new type of MZ modulator which provides many advantages compared to other contemporary optical modulator technologies available, and is a comparable alternative to established LiNbO$_3$ MZ

modulators, because of their small physical size [3] and low Power consumption [4], potential for parallel modulator architectures [5, 6] and monolithic integration capability with other laser components [7]. Utilizing the Quantum Confined Stark Effect (QCSE) in a semiconductor MQW enables a small physical size modulator to be realized with comparatively low drive voltage and low power consumption, enabling multi-component integration [8] with other commercially available chip technologies, providing additional enhanced functions, but without significant manufacturing cost penalties. However application of InP MZ modulator is still at its infancy, and related technologies and models of InP based optical devices are presently under development for practical applications. To support the evaluation of a new modulator technology, opto systems designers must first be able to accurately model and predict the performance of the component within the optical network, prior to committing financial and human resources and unnecessary installation. It is therefore necessary to develop a model capable of accurately simulating the practical performance of the component under test. This paper discusses the development of an InP MZ modulator model. InP MZ modulator chip have been designed and fabricated. The key modulator parameters such as optical extinction ratio and chirp were measured and extracted. Resultant model-derived and practical measurements are compared against the more mature and well established

Lithium Niobate (LiNbO$_3$) material based Linear Electro Optic (LEO) MZ modulator.

2. Analytical model

2.1 Principle of MZ-modulator

Modeling the dynamic performance of an optical modulator within a telecommunications network is an important activity in designing and commissioning high performance optical systems. In order to carry out the modeling, analytical models related to each physical phenomenon will be developed in this section.

MZ modulators are a key component to enable higher modulation speeds, larger ON/OFF (optical extinction) ratios, and low/controllable frequency chirp. An MZ optical modulator uses an interferometric configuration of waveguides to enable the conversion of phase modulation into intensity modulation through two branches of waveguide. When the continuous wave laser source signal is first split into the two waveguides, a relative phase difference $\Delta\phi$ is introduced at the combining branch through an electro-optic effect, and then recombined at the output Y branch of the modulator as shown in Figure1. When the phase shift $\Delta\phi$ between the two arms equals $\pm\pi$, destructive interference occurs, corresponding to the off-state or "0" level for the modulator. With no phase shift, $\Delta\phi$=0, constructive interference occurs, corresponding to the on-state or "1" level for the modulator. Current established MZ modulators are typically based on LiNbO$_3$ or GaAs. The phase difference $\Delta\phi$ is introduced through the Linear Electro-Optic (LEO) or Pockels effect. The LEO relationship between the applied electric field acting on the waveguide, the subsequent change in material refractive index of the waveguide and resultant change in phase of the optical energy travelling through the waveguide is defined in Eq.1, [9].

$$\Delta\phi = \frac{2\pi n_O r V}{S\lambda_O} \quad (1)$$

where r is the electro-optic constant of the material measured in meters per applied volts (m/V), n_o is the refractive index of the material with no bias applied, S is the electric field interaction depth, and λ_o is the wavelength of the applied optical energy under influence travelling through the waveguide.

The LEO MZ modulator output-intensity P_{out} versus applied voltage V characteristic can be expressed in terms of a raised cosine function of the relative phase or applied modulation voltage as shown by Eq.2, [10, 11].

$$P_{out} = P_{in}\left(\cos^2\left(\frac{\Delta\phi}{2}\right)\right) = P_{in}\left(\cos^2\left(\frac{V}{V_\pi} + \sigma\right)\right) \quad (2)$$

Where P_{in} is the input optical intensity, $V_\pi = \pi/cl$ is the magnitude of voltage required to produce a relative π

phase shift change between the two waveguides of the MZ modulator and change the output light intensity from its maximum value to its minimum value, c is a constant related to the material electro-optic coefficient, refractive index and the geometries, l the active electrode length (shown shaded in fig.1) and σ is a static phase shift fabricated within one of the waveguides of a practical modulator.
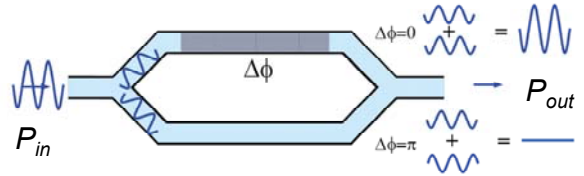

Fig. 1. Schematic drawing of a Mach-Zehnder (Phase) Modulator.

2.2 InP MZ Modulator

The InP MZ modulator typically has the same dual waveguides and Y branch structure as the conventional LEO MZ modulator as shown in Fig.1. The fundamental difference for the InP MZ is that optical modulation is achieved by fabricating Multi-Quantum Well structures (MQWs) within the two MZ modulator waveguides. The addition of the MQWs enables a highly efficient MZ (phase engineered) modulator to be realized utilizing the Quantum Confined Stark Effect (QCSE) [12, 13] induces strong material refractive index changes within the modulator arms through the Kramers-Kronig relation.

The Stark Effect originates from the interaction between a charge distribution (atom or molecule) and an external applied electric field. In a heterostructure, where a small bandgap material is sandwiched between two layers of a larger bandgap material, the Stark effect can be greatly enhanced by bound excitons. The electron-hole pair which form the exciton are pulled in opposite directions by the applied electric field, but remained confined in the smaller bandgap material, so the exciton is not pulled apart by the field [14].

The QCSE lends itself well for semiconductor based electro-absorption modulators [15], as the amount of photon absorption has a non-linear relationship with the applied electric field. The relation between the change in material refractive index and the QCSE change in material absorption caused by excitation of a medium is related to the Kramers-Kronig relation [12, 13]. The resultant Phase shift depends on the relative wavelength detuning, λ_D between the operating wavelength λ_o and the material exciton peak absorption wavelength λ_e at 0V [16]. Larger detuning is required compared to a pure electro-absorption modulator [15], to reduce the effects of absorption. Typical λ_D is between 120nm-175nm depending on the application and operational wavelength [16].

$$\Delta n_{(\lambda 0)} \propto \int \frac{\Delta\alpha_\lambda}{\lambda_o{}^2 - \lambda_e{}^2} d\lambda \quad (3)$$

where $\Delta\alpha$ is the material absorption coefficient change with applied voltage, Δn is the resultant material refractive index change, λ_e is the exciton peak absorption wavelength, λ_o is the operating wavelength.

The light intensity output versus applied bias voltage is one of the most important parameters for InP MZ modulator model. However the material absorption effects and non-linear phase characteristic of the InP MZ modulator make the development of a model much more complex than an LEO MZ modulator. The modulator attenuation per modulator waveguide versus applied voltage can be estimated from the material absorption coefficient;

$$A_{(V)} = 1 - \exp^{-\alpha(V)} \qquad (4)$$

Similar to the conventional LEO MZ modulator, the modulated optical output power intensity is the sum of the two phase modulated intensities. The output power intensity is influenced by the optical split and combining ratios of the MZ modulator and the independently applied bias voltages. The relationship of phase change $\Delta\phi$ with the applied voltage is linear for LiNbO$_3$ or GaAs based MZ modulators, but non-linear for a InP MZ modulator due to the QCSE effect. The optical output is then modified as shown by Eq.5.

$$P_{out} = \left[\sqrt{A}\cdot\exp\left(\frac{-\alpha_{(VL)}}{2}-i\left(\Delta\phi_{(VL)}+\delta_L\right) \right) + \sqrt{B}\cdot\exp\left(\frac{-\alpha_{(VR)}}{2}-i\left(\Delta\phi_{(VR)}+\delta_R\right) \right) \right]^2 \qquad (5)$$

where A and B can be either the optical splitting ratios or electric field splitting ratios of the modulator Y branches.

The zero voltage phase imbalance terms δ_L and δ_R are the phase offsets in each of the waveguide arms respectively, δ_L is π and δ_R is zero for a practical MZ modulator fabricated to produce zero output with zero applied voltage, while δ_L is $\pi/2$ and δ_R zero for a practical MZ modulator fabricated to produce half-power output with zero applied voltage.

The phase change $\Delta\phi$ in radians is directly related to applied bias voltage V and is related to the modulator waveguide length l and wavelength detuning coefficient λ_D [17].

$$\Delta\phi = l\cdot\left(p_1|V| + p_2|V|^2 \right) \qquad (6)$$

$$\alpha = a_1|V|^{a2} \qquad (7)$$

where p_1, p_2 and a_1, a_2 are empirically derived constants related to λ_D [17].

The efficiency of an MZ optical modulator is quantified by its extinction ratio (ER), which is defined as the ratio of optical power of the on-state to the off-state. For a perfect symmetrical modulator the extinction ratio

would be infinite, however practical device with fabrication variation in the length, the split and combining ratios, non-linearity effect and finite switching (modulation bandwidth) etc. result in a finite value of ER, and can be estimated as follows.

$$ER = \left(\frac{A + B + 2(AB)^{1/2}}{A + B - 2(AB)^{1/2}} \right) \qquad (8)$$

To realize a high efficiency electro-optic conversion and resultant low power dissipation and low V_π drive voltages for an InP MZ modulator, it is necessary to match the speed of the energizing electric field travelling along the electrodes with the velocity of the light through the waveguides [18, 19]. If the RF phase velocity and the optical group velocity are well matched then the modulation group will maintain its phase relationship. By increasing the interaction length and implementing velocity matching to improve electrical and optical wave confinement of the electrical and optical signals, V_π voltages are reduced and modulation bandwidth increased [20]. The resultant InP MZ modulation electro-optic bandwidth is typically 13GHz [21], suitable for current 10Gb/s telecommunications applications.

2.3 Optical component transient behavior

To enable accurate modeling of the InP MZ modulator within an optical system, it is necessary to consider the transmission medium over which the optical information will be transmitted. Optical fibre chromatic dispersion is a phenomenon associated with optical fibres which can severely degrade Quality of Service (QOS) and can limit data transmission speed and distance. Chromatic dispersion results in broadening of the input signal as it travels down the length of the fibre. The global deployment of DWDM systems operating over wide operating wavelength bands and higher speed operation, require the effects of chromatic dispersion to be considered.

The optical fiber is essentially a waveguide with a fiber core of refractive index n_1 surrounded by a secondary core of refractive index n_2, where $n_1 > n_2$. There are two major causes of chromatic dispersion: material dispersion and light distribution across the fiber. All optical signals have a finite spectral width, and different spectral components will propagate at different velocities along the length of the fiber. The velocity difference is primarily due to the index of refraction of the fiber core being different for different wavelengths. This is the dominant source of chromatic dispersion in single-mode fibers. Another cause of dispersion is that the cross-sectional distribution of light within a fiber also changes for different wavelengths. Shorter wavelengths are more completely confined to the fiber core, while a larger portion of the optical power at longer wavelengths propagates in the cladding. Since the index of the core is greater than the index of the cladding, this difference in spatial distribution causes a change in

propagation velocity and temporal broadening of the propagating optical pulse.

The dispersion properties of a Single Mode optical Fibre (SMF) can be defined by its dispersion slope, D_λ and is specified in picoseconds per nanometer-kilometre (ps/nm.km) [22].

$$D_\lambda = \frac{S_0}{4}\left(\lambda - \frac{\lambda_S^4}{\lambda^3}\right) \qquad (9)$$

Where λ is the operating wavelength, λ_S is the minimum dispersion wavelength and S_0 is the dispersion slope at the minimum dispersion wavelength. The amount of pulse broadening can be quantified considering the fibre and optical modulator properties. The broadened optical pulse width $\tau_{(L)}$ with respect to the initial pulse width τ_0 can be estimated [22].

$$\tau_{(L)} = \tau_0 \sqrt{\left(1 + \left(\frac{\Phi D_\lambda L}{\tau_0^2}\right) + \left(\frac{D_\lambda L}{\tau_0^2}\right)^2\right)} \qquad (10)$$

Where L is the fiber length in km, D_λ is the fibre dispersion slope as defined above and Φ the MZ modulator line enhancement parameter.

Another phenomenon associated with all optical modulator technologies is the generation of frequency transients (commonly called Chirp) during switching of the modulator between ON and OFF states. Chirp has a significant effect on high speed optical system performance and hence has been a subject of significant research [23, 24 & 25]. The transient frequency $v_{(t)}$, during the modulator state transition can be considered as a temporal derivative of the change in phase, $d\phi/dt$, of the propagating optical energy within the MZ modulator waveguides.

$$v_{(t)} = \frac{1}{2\pi}\frac{d\phi}{dt} \qquad (11)$$

Optical modulators are typically defined as being positive or negative or zero chirped. With negative chirp, a negative transient frequency (positive wavelength shift) occurs during the off=>on modulator state change, and a positive transient frequency (negative wavelength shift) occurs during the on=>off modulator state change. Zero-chirped modulators produce minimal chirp during the switching transition, while negative chirped modulators are primarily used to overcome the effects of fiber dispersion.

Chirp must be considered when designing high performance high speed optical systems. Since negatively chirped MZ modulators reduce the effects of fiber chromatic dispersion and maintain the optical pulse shape over an extended fiber length. Effects of optical pulse dispersion and resultant reduction in system quality of service can be estimated, based on the modulator alpha parameter, operational wavelength, bit rate and fiber length and fiber chromatic dispersion coefficient [26].

The chirp performance of an optical modulator is more often defined in terms of a small signal line enhancement parameter, which relates the change in phase to the change in intensity of the modulated optical energy. The line enhancement parameter Φ can be used to estimate the optical pulse spreading as it propagates through an optical fiber [22].

$$\Phi = 2I\left|\frac{\frac{d\phi}{dt}}{\frac{dI}{dt}}\right| \qquad (12)$$

where I is the instantaneous optical power intensity measured at half maximum.

Engineering the chirp performance and line enhancement parameter to suit the telecommunications system application is thus critical. This has been achieved in Lithium Niobate modulators by optimizing the modulating electric field ratios (E_R & E_L) acting on the two identical modulator waveguide branches. The modulating electric field ratios acting on the waveguide branches are of the same magnitude for the InP modulator with the required chirp performance achieved during the InP MZ chip fabrication process by non-symmetric optical split and combining ratios (A & B) within the Y branches. In both cases the two modulating electric fields are applied differentially (in anti-phase).

$$\Phi_{LiNbO_3} \approx \frac{E_R + E_L}{E_R - E_L} \qquad (13)$$

$$\Phi_{InP} \approx \frac{A - B}{A + B} \qquad (14)$$

Practical experimentations have identified the optimum line enhancement parameter for an LEO MZ optical modulator to be approximately $\Phi=-0.7$ for a point-to-point optical fibre link length of 80 to 120km [27]. However the InP MZ optimum line enhancement parameter is $\Phi=-0.4$, the difference compared to the LEO modulator is due to the non-linear phase versus light-out characteristic of the InP MZ modulator.

Figs. 2a shows diagrammatically the definition of chirp. The definition of negative chirp when referring to Eq.12 implies a negative phase and thus negative frequency excursion for a positive optical power excursion, and vice versa. Negative chirp counteracts the effects of optical fiber dispersion. (b) shows the practical modulated optical power intensity and chirp behavior for an InP MZ modulator, which in this case is clearly negative chirped. The measurement was performed using a commercially available Advantest Optical Chirp Test Set Module, Q7607, which measures optical power intensity and optical frequency deviation in the time domain [28].
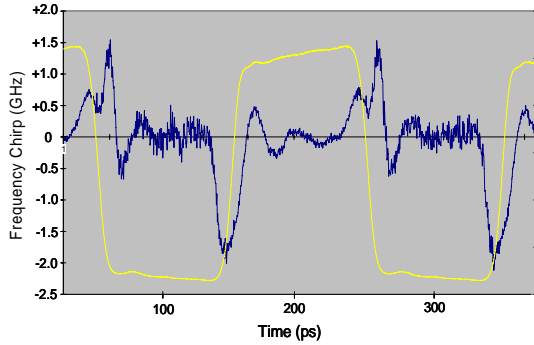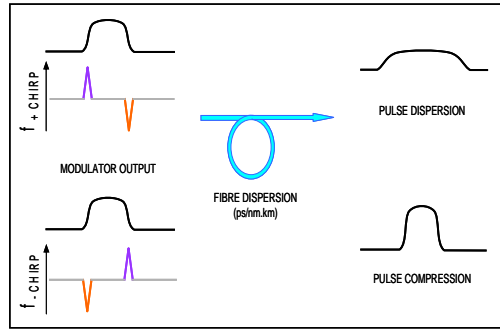
Fig. 2a, Chirp Definition & Pulse Shape Representation over a Dispersive Medium, (b) Practical InP MZ Negative Chirp Measurement.

3.4 System Performance

A parameter associated with optical system performance and overall quality of service (QOS) is the system Bit-Error Rate (BER) which can be measured and modeled. Considering serial transmission of digital optical pulses, propagating along a dispersive medium (fiber) and being received at the optical receiver, it is important that the pulses are correctly detected and electrically regenerated. The BER of a system can be estimated fairly simply using Gaussian noise statistically analysis [29] by considering the signal to noise ratio (SNR_E) or Q factor of an electrically regenerated digital signal following opto-electric conversion by an optical receiver [29]. A penalty in optical systems performance can then be estimated and compared to practical optical systems measurements performed over a non-ideal transmissions medium such as optical fibre [29].

$$BER = \frac{1}{2}\left[erfc\left(\frac{\mu_1 - V_{DL}}{\sigma_1} \right) + erfc\left(\frac{V_{DL} - \mu_0}{\sigma_0} \right) \right] \quad (15)$$

$$Q = \frac{|\mu_1 - \mu_0|}{|\sigma_{1} + \sigma_0|} \quad (16)$$

where, μ_1 is the mean optical signal power detected by the optical receiver for a one state and μ_0 is the mean optical signal power detected by the optical receiver for a zero state, σ_1 and σ_0 are the measured standard deviations of the noise distributions superimposed onto the detected digital one's and zero's signal levels respectively. V_{DL} is the digital decision threshold of the post opto-receiver electrical flip flop, typically set midway between μ_1 and μ_0. The parameters identified in Eq's 15 & 16 can conveniently be measured using commercially available telecommunications test equipment, such as an Optical Communications Analyser. For the simulation, a BER Meter block is developed which also performs a statistical analysis on the generated results matrix, estimating the mean and standard deviations prior to deriving a BER value using the *erfc* function.

Simulating the dynamic performance of an optical modulator within a telecommunications network is an important activity in the design and commissioning of high performance systems. The parameters previously identified can be used to build a model of an optical modulator using commercially available software suits such as MATLAB™ and VIRTUAL PHOTONICS™. Figure 3 shows the Simulink system. Generic Simulink library blocks were used for the pulse train PRBS generator and Butterworth filter. The Butterworth filter was used to provide a finite bandwidth of 13GHz representative of a practical InP MZ modulator. Two gain blocks were used to provide the required differential drive voltage for the modulator. The optical fiber chromatic dispersion characteristic was modeled using the equivalent of a discrete "all pass" filter that changed only the temporal phase of the signal versus it's frequency as defined in Eq.9, Eq.10 & Eq.11, with D_λ = 16.26 ps/(nm.km), λ_S = 1302nm, S_0 = 0.092 ps/(nm².km). An InP MZ model was built using the MZ modulation transfer characteristics detailed in Eq.5, Eq.6 & Eq7. The MZ constants were estimated empirically using current production-line sample: p_1=2.73e⁻⁴, p_2=4.20e⁻⁵, a_1=0.049, a_2=1.025, when λ_o=1550.50nm and λ_D =125nm. The dimensions, waveguide length (l =3mm) and other physical parameters of the modulator were taken from the actual devices made as described in the next section. The InP MZ model parameters and optical fiber transmission properties are summarized in table 1.

Table 1. InP MZ model parameters and fiber transmission properties.

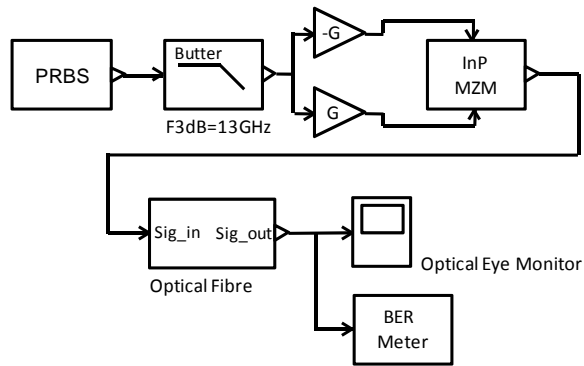| InP MZ Model				Optical Fibre Model
λ_e = 1425.5 nm	λ_D = 125 nm	λ_o = 1550.5 nm	F_{3dB} = 13GHz	D_λ = 16.26 ps/(nm.km)
p_1 = 2.73e⁻⁴	p_2 = 4.20e⁻⁵	a_1 = 0.049	a_2 = 1.025	λ_S = 1302 nm
A = 57:43	B = 57:43	δ_L = 0	δ_R = π/2	S_0 = 0.092 ps/(nm².km)
				λ = 1550.5 nm

Fig. 3. Simulink optical system model.

3. Device fabrication and testing system

A practical realization of an InP MZ modulator chip is shown in figure 4, and is 500μm wide and 4mm in length with the electrical modulation voltage applied via dual independently driven 2μm wide by 1.5mm long micro strip waveguide (modulator) electrodes. The InP MZ modulator optical phase modulated waveguides influenced by the applied electric fields are 285um straight with a lateral width of 1.5um and fabricated with a strongly guided P-I-N doped cross section providing optimum electro-optic conversion efficiency. The intrinsic region contains thirty one 95Å InGaAsP wells and thirty two 80Å InGaAsP barriers. The guided mode is highly confined to the MQW core, enabling good overlap efficiency with the large electric field that can be created across the thin intrinsic region. In the modulator waveguides the QCSE convert the applied electrode field into an effective refractive index change and hence an optical phase shift to the propagating mode. The InP MZ must always be negatively biased to ensure the P-I-N structure does not conduct.
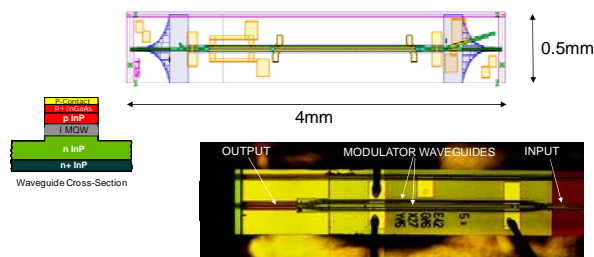

Fig. 4. InP MZ waveguide cross section, chip layout and fabricated modulator.

The test conditions used (both simulated and practical measured) were with the modulator being modulated at 10Gb/s with a Pseudo random (PRBS), non-return to zero (NRZ) bit sequence. For this exercise the InP MZ has been fabricated with non-symmetric splitting and combining

ratios as discussed to generate negative chirp and a line enhancement factor, Φ of -0.4, resulting in pulse compression of the optical pulse through fiber. An LEO LiNbO$_3$ MZ modulator was also measured for comparison. The LiNbO$_3$ modulator selected, type; F10-Z-PowerBit™ negatively chirped, is a commercially available modulator [30]. Figure 5 shows the test setup used to measure the modulator eye shapes.
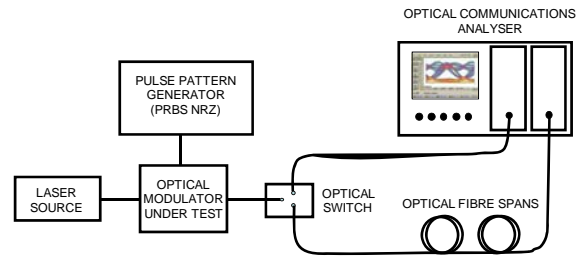

Fig. 5. Optical modulator test equipment.

4. Results and discussion

Fig. 6a shows a typical InP MZ modulator absorption characteristic versus wavelength, and (b) shows a typical phase and absorption characteristic at λ_o =1550.50nm for the same modulator. The increase in absorption and resultant non-linear phase characteristic as the bias voltage increases due to the Quantum confined Stark effect as described by Eq.4, Eq.6 & Eq.7 can be clearly seen. The modulator fitting parameters; p_1, p_2, a_1, & a_2, identified in Eq.6 & Eq.7 can be derived from these profiles and used to model the overall modulator transfer function shown in Eq.5. Also shown in (b) is a typical LiNbO$_3$ LEO MZ modulator absorption and phase characteristic, It can be seen that the LiNbO$_3$ MZ has constant absorption with applied voltage and also a linear phase characteristic, hence why LiNbO$_3$ material based MZ modulator are known as a Linear-Electro-Optic (LEO) modulators. The InP MZ modulator is typically biased at a low voltage (low applied MZ waveguide bias voltages ~ -2V$_{DC}$) to obtain the lowest absorption per radian of phase shift and produces the most linear phase change per volt of reverse bias, therefore resembling an LEO modulator. The resultant advantage of the InP MZ modulator is that the equivalent magnitude of phase change can be realized with a significantly smaller physical size of modulator chip. (c) shows the variation in InP modulator waveguide absorption and relative phase shift characteristic versus wavelength λ_o. The absorption characteristic, α described in Eq.6 and phase characteristic, $\Delta\phi$ described in Eq.7 are directly related to the value of relative wavelength detuning, λ_D as described in Eq.3.
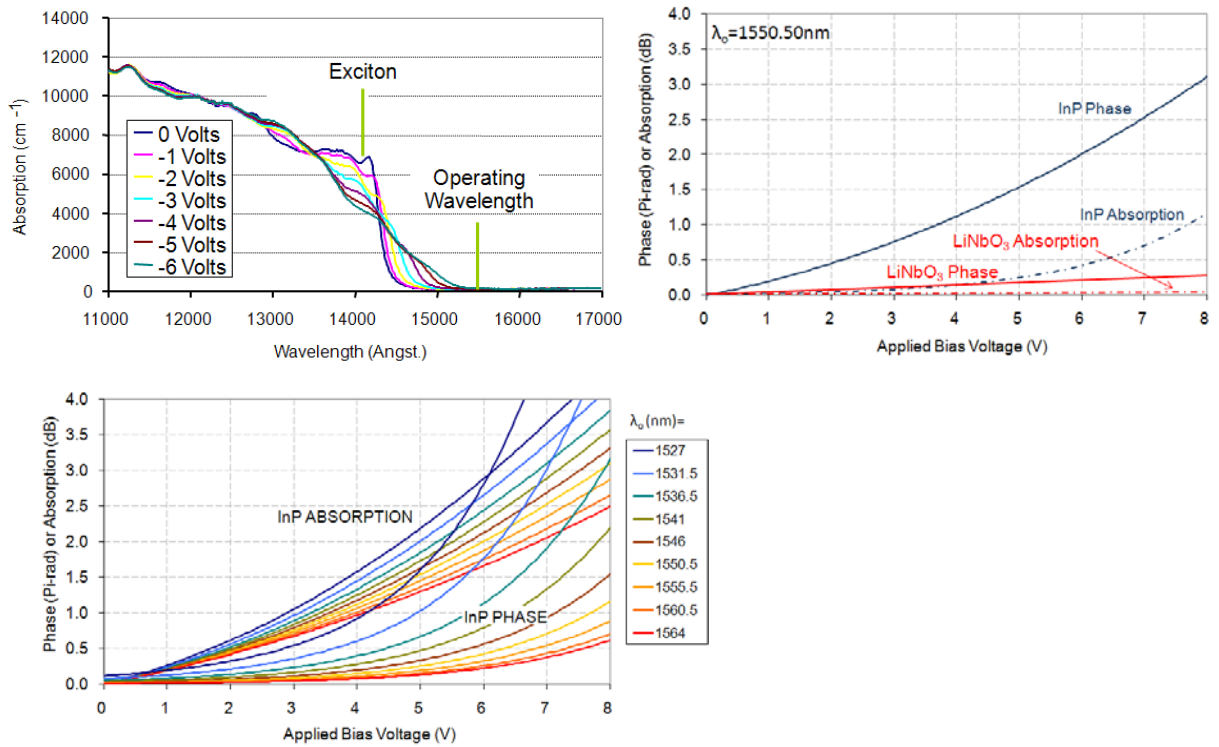
Fig. 6a is the InP absorption profile versus wavelength with λ_e and λ_o identified, $\lambda_{D \; is}$ ~125nm. (b) shows a typical phase and absorption profile for both an InP and LiNbO$_3$ material based MZ modulator at λ_o =1550.50nm. (c) shows the variation in InP absorption and relative phase shift with versus wavelength λ_o.

A typical InP MZ modulator light output P_{out}, versus bias voltage applied to each of the modulator waveguides is shown in Figure 7, each waveguide is driven independently, (a) shows a color grade scale of output power P_{out}, with both voltages applied to the modulator waveguides independently, (b) is the output power profile when only one modulator waveguide, in this case the right waveguide is swept with an applied voltage, the non-linear relationship and effects of absorption can be seen

clearly as the output power diminishes with deeper bias voltage, and is typical of a QCSE phase-modulated optical MZ modulator. By applying different voltage to each of the waveguides, it is possible to achieve an optical output at any value between the maximum and minimum values shown. For comparison, an LEO modulator profile is also shown in (b), it can be seen that the LEO modulator has the typical cyclic raised cosine profile with applied voltage, as described in Eq.2.
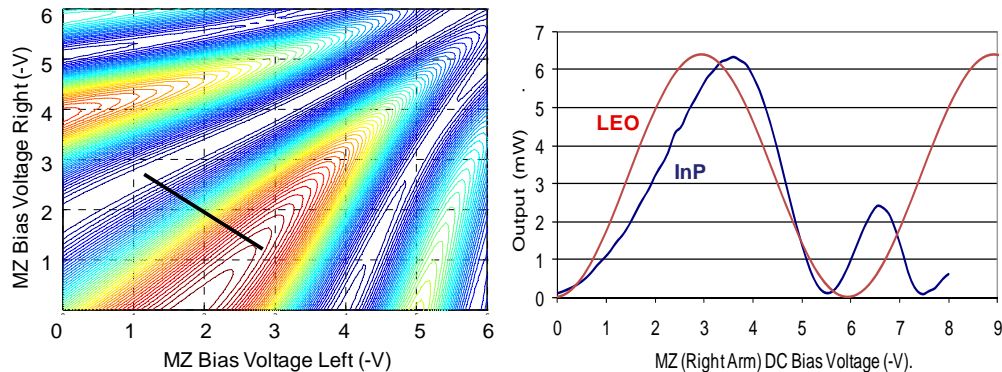

Fig. 7. InP MZ Light versus Voltage Profiles.

Fig. 8 shows the comparison of simulated and measured results for a modulator with no optical fiber dispersion, and Fig. 9 is the comparison of the simulated and measured results for the modulator with an addition of chromatic dispersion equivalent to 80km of single mode optical fiber, approximately 1600ps/nm. The x-axes for all figures have the same time scale, the y-axis is optical intensity, P_{out}. When the chromatic dispersion is considered in the system, the amplitudes of the transmission showed some degree of dispersion, and is clearly reflected in the simulated results for the InP MZ modulator. For both system scenarios considered, with and without chromatic dispersion, the simulated results showed very identical behavior to the practical results measured, indicating the accuracy of the models developed, and the eye shape is also similar to that from a commercially available LiNbO$_3$ MZ modulator, demonstrating the feasibility of the InP MZ modulator as a physically compact alternative modulator technology to the benchmark LiNbO$_3$ material based modulator.

(a) InP MZ Simulation   **(b) InP MZ Measured**   **(c) Benchmark LiNbO3 LEO MZ**
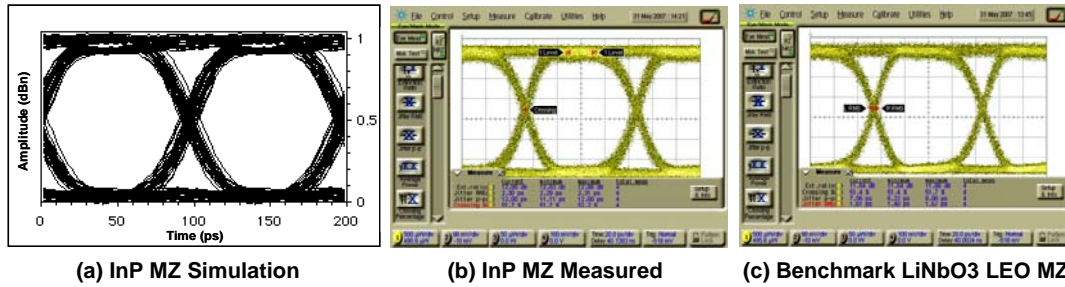
Fig. 8. Modulated Optical Eye Shapes with no optical fiber dispersion: (a) InP MZ Modulator Simulation, (b) InP MZ Modulator Practical Measurement, (c) Benchmark LiNbO$_3$ LEO Modulator Practical Measurement.

(a) InP MZ Simulation   **(b) InP MZ Measured**   **(c) Benchmark LiNbO3 LEO MZ**
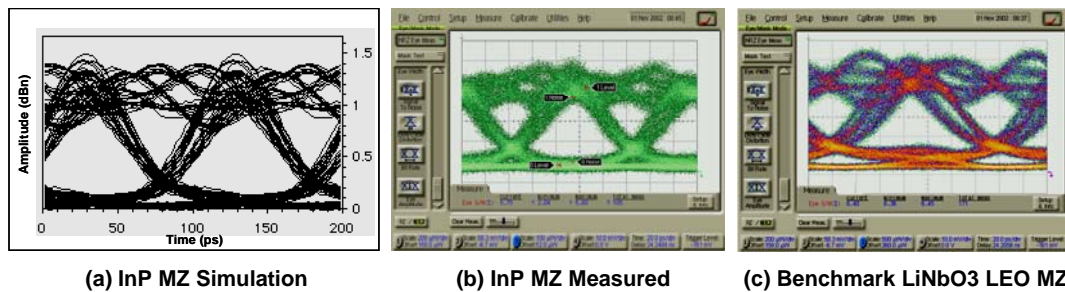
Fig. 9. Modulated Optical Eye Shapes with optical fiber dispersion considered: (a) InP MZ Modulator Simulation, (b) InP MZ Modulator Practical Measurement, (c) Benchmark LiNbO$_3$ LEO Modulator Practical Measurement.

Fig. 10 is a comparison of the simulated and measured InP modulator performance operating at 10.709Gb/s with a PRBS NRZ data pattern. The optical systems penalty, defined as the change in optical power at the optical receiver to maintain a BER of 10^{-10} (only one error in every $1e^{10}$ data bits), measured in an optical system with variable fibre length and hence variable fibre dispersion parameter D_λ. The InP MZ optical systems performance in terms of a power penalty due to optical fibre induced pulse dispersion shows good agreement with the model simulated results. An LiNbO$_3$ modulator is shown for comparison. The results demonstrated that InP MZ modulator has a comparable performance to that of an liNbO$_3$ MZ modulator when operated at 10.709Gb/s.
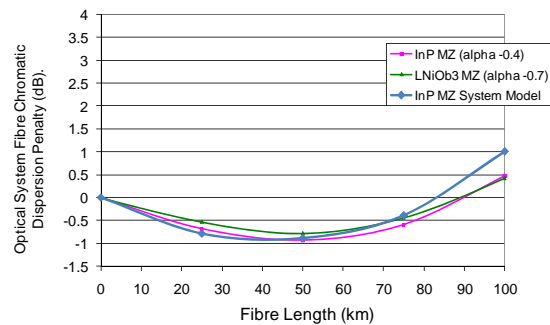

Fig. 10. Modulator Technology Optical System Penalty Comparison due to Chromatic Dispersion, 10.709Gb/s, NRZ PRBS 2^{23}-1 data, λ=1530nm, D=16ps/nm.km.

The modeled versus practical measurements of the InP MZ optical modulated eye shape and in-system dispersion penalty performance show good agreement, and the InP MZ systems showed similar performance to the well established LEO LiNbO$_3$ MZ modulator, demonstrating it is feasible that the developed model can be used for optical system simulation purposes, and InP MZ modulator can be used to replace the LiNbO$_3$ MZ modulator for better integration.

The small physical size of the InP MZ modulator enables it to be used as a building block for further photonic integration. Research and development is presently ongoing to realize multi-component (hybrid) integrated photonic transmitter components which include InP optical beam guides, providing the optical connection between individual components [31], enabling integrated photonic components which include parallel modulator architectures to support the continued demand for domestic broad band and internet services.

An active area of research is realizing an optical modulator capable of 40Gb/s operation. Higher speed operation typically requires a reduction in pulse/bit period which produces an increased transmission penalty, because the effects of optical fiber chromatic dispersion and other non-linear effects associated with fiber-optic transmission mediums increase significantly. For example a 10Gb/s pulse width is 100 ps and at 40Gb/s is only 25ps,
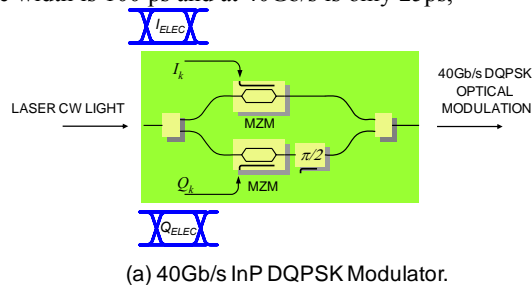
therefore any degradation of pulse shape of only a few picoseconds can significantly affect optical system BER and QOS [32].

Simply scaling the speed of current (10Gb/s) NRZ modulators upwards is not possible, as the required increase in electro-optic modulator bandwidth cannot easily be achieved. Therefore the use of spectrally efficient modulation schemes such as DPSK and DQPSK are currently being investigated for both 40Gb/s and 100Gb/s. For example DQPSK provides a spectral efficiency of 1.6b/s/Hz, versus current NRZ which is 1b/s/Hz, providing an immediate increase in potential transmission speed of 60% without having to change the existing optical network topology. Orthogonal DQPSK has recently been proven to provide spectral efficiencies up to 3.2b/s/Hz [33]. Therefore DQPSK is increasingly being considered as an upgrade option for existing optical networks and DQPSK modulator architectures are being evaluated [34, 35] as shown in Fig. 11.

The InP MZ modulator and model described in this paper provides the building block required to support these evolving integrated modulator designs using parallel optical modulator integration techniques. Monolithic integration of the InP MZ with laser technologies is also progressing and initial results are encouraging [36].

(a) 40Gb/s InP DQPSK Modulator.
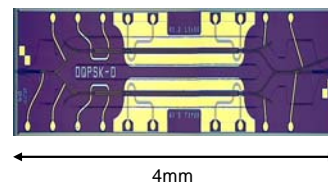
(b) Proposed InP MZ Parallel DQPSK Chip Layout.

Fig. 11a, 40Gb/s InP DQPSK Modulator Block Diagram. (b), Proposed InP MZ Parallel DQPSK Modulator Chip Layout.

5. Conclusions

The development of an InP MZ model enables system designers to evaluate and confirm fit for purpose prior to committing significant financial or engineering resources. The use of the model therefore reduces technical risk and provides confidence in the capabilities of this emerging technology. The relatively small physical size of the InP MZ modulator enables multi-component integration with other photonic technologies such as tunable lasers. The small physical size of the InP MZ modulator allows the realization of parallel modulator structures, not easily supported by LEO (LiNbO$_3$) type modulators, enabling more advanced spectrally efficient modulation schemes for higher data through-put. The InP MZ modulator and model are ideal building blocks for optical system designers to simulate the potential of the modulator for use in current optical system networks as an alternative to the physically larger LEO modulators and supports new

emerging photonically integrated components for advanced applications.

References

[1] F.J. Leonberger, Opt. Lett. **5**, 312, (1980)
[2] J.P. Donnelly, N. L. DoMeo, G.A. Ferrante, K.B. Nichols, F.J. O'Donnel, Appl. Phys. Lett. **45**, 360 (1984)
[3] B. Hitz, Optics Express, **10**, 17106 (2007).
[4] K. Tsuzuki et al, Optical Fiber Communication Conference, Vol. 2, 2004.
[5] T. Ye et al, Optics Communications, **281**, pp. 4648–4652, 2008.
[6] H. Chi, X. Zhang, J. Yao, Optics Communications, **281**, 2517 (2008).
[7] J.S. Barton, E.J. Skogen, M.L. Masanovic, S.P. DenBaars, IEEE Journal of Selected Topics in Quantum Electronics, 2003.

[8] H. Debrégeas-Sillard, C. Kazmierski, C. R. Physique, **9**, 1055 (2008).

[9] H. Jin, M. Belanger, Z. Jakubczyk, IEEE Journal of Quantum Electronics, **27**(2), 243 (1991).

[10] B.H. Kolner, D. W. Dolfi, Applied Optics, **26**, 3676 (1987).

[11] J. L. Brooks, G. S. Maurer, R. A. Becker, Journal of Lightwave Technology **11**, 34 (1993).

[12] M.Sheik-Bahae, Enc. of Modern Optics, Academic Press, London, 2004.

[13] K. Tada, T. Arakawa, J-H. Noh, N. Haneji, IPAP Books **2**, 199 (2005).

[14] W.Y. Liang, Phys. Educ, **5**, 226 (1970).

[15] H. Debregeas-Sillard, et al, IEEE Photonics Technology Letters, **11**(11), 1485 (1999).

[16] W. Bardyszewski, D. Yevick, Y. Liu, C. Rolland, S. Bradshaw, J. App. Phys, **80**(2), 1136 (1996).

[17] I. Betty et al, Optical Fiber Communication Conference, pp. 3, Vol. 3, 2005.

[18] W. Pascher et al, Opt. and Quant. El, 2003.

[19] D. Caprioli et al, 11th Eur. Conf. on Int. Opt. (ECIO '03), pp, 145–148, April 2–4 2003.

[20] D. Janner, D. Tulli, M. Belmonte, V, Pruneri, J. Opt. A: Pure Appl. Opt. **10**, 104003 (2008).

[21] Le Nguyen Binh, I. J. Communications, Networks and System Sciences, **2**, 91 (2009).

[22] K. Thyagarajan, "An Introduction to Fibre Optics," Cambridge University Press, 1998.

[23] T. Ohtoshi, Topics in Quantum Electronics, **9**(3), 755 (2003).

[24] K. Prosyk, R. Moore, et al, OFC 1, pp. 269 (2003).

[25] P. Bravetti et al, Journal of Lightwave Technology, **22**(2), 605 (2004).

[26] Agrawal, P. Govind, "Fiber-Optic Communication Systems, Second Ed. Wiley Series in Microwave and Optical Engineering, 1997.

[27] A. H. Gnauck, et al, Photonics Technology Letters, IEEE, **3**(10), 916 (1991).

[28] R. A. Saunders, J.P. King, I. Hardcastle, Electronics Letters, **30**(16), 1336 (1994).

[29] I.P. Kaminow, T.L. Koch, Optical Fiber Communications III, Vol. A, Academic Press, pp. 314-318, 1997.

[30] http://www.oclaro.com/product_pages/ Powerbit_XS10-Z.html, D2801 PowerBit XS10-Z Version 1.1 September 2009.

[31] R. Nagarajan et al, IEEE Journal, Selected Topics in Quantum Physics, **11**(1), 50 (2005).

[32] J. Wang and J.M. Kahn, J. Lightwave Technology. **22**, 362 (2004).

[33] F.C.G. Gunning, T. Healy, X. Yang, A.D. Ellis, Lasers and Electro-Optics, 2007 and the International Quantum Electronics Conference. CLEOE-IQEC 2007. European Conference on Optical Communications (ECOC), pp. 1, June 2007.

[34] D. Van Den Borne, S.L.Jansen, E. Gottwald, E, E.D. Schmidt, E.D, G.D. Khoe, G.D, H. de Waardt, Optical Fiber communication/National Fiber Optic Engineers Conference, 2008. OFC/NFOEC 2008, pp, 1 – 3, Feb. 2008.

[35] T. Yasui, Y. Shibata, K. Tsuzuki, N. Kikuchi, Y. Kawaguchi, Y. M. Arai, H. Yasaka, Optical Fiber communication/National Fiber Optic Engineers Conference, 2008. OFC/NFOEC 2008. European Conference on Optical Communications, pp, 1-3, Feb. 2008.

[36] D.J. Robbins, Lasers and Electro-Optics 2007, CLEO 2007, pp, 1-2, May 2007.

_____
[*]Corresponding author: Philip.Mitchell@oclaro.com